The Vibrational Spectrum of α-AlOOH Diaspore: An Ab Initio Study with the CRYSTAL Code

R. Demichelis,[†] Y. Noel,[‡] B. Civalleri,[†] C. Roetti,[†] M. Ferrero,[†] and R. Dovesi*[,§]

Dipartimento di Chimica IFM, Università di Torino, Via P. Giuria 7, 10125 Torino, Italy, Université Pierre et Marie Curie—Paris6, UMR 7160, Lab. PMMP, Paris 75005, France, and Dipartimento di Chimica IFM, Università di Torino and NIS (Nanostructured Interfaces and Surfaces, Centre of Excellence, http://www.nis.unito.it), Via P. Giuria 7, 10125 Torino, Italy

Received: March 30, 2007; In Final Form: May 23, 2007

The vibrational spectrum of α-AlOOH diaspore has been calculated at the B3LYP level of theory with a double-ζ quality Gaussian-type basis set by using the periodic ab initio CRYSTAL code. Harmonic frequencies at the Γ point and the corresponding 48 normal modes are analyzed and classified in terms of simple models (octahedra modes, hydrogen stretching, bending, rotations) by direct inspection of eigenvectors, graphical representation, and isotopic substitution. Hydrogen modes are fully separated from the octahedra modes appearing under 800 cm^{-1}; bending modes are located in the range of 1040−1290 cm^{-1}, whereas stretching modes appear at 3130−3170 cm^{-1}. The available experimental IR and Raman spectra are characterized by broad bands, in some cases as large as 800 cm^{-1}, and individual peaks are obtained by decomposing these bands in terms of Lorentz−Gauss product functions; such a fitting procedure is affected by a relatively large degree of arbitrariness. The comparison of our calculated data with the most complete sets of experimental data shows, nevertheless, a relatively good agreement for all but the H modes; the mean absolute differences for modes not involving H are 10.9 and 7.2 cm^{-1} for the IR and the Raman spectra, respectively, the maximum differences being 15.5 and 18.2 cm^{-1}. For the H bending modes, differences increase to 30 and 37 cm^{-1}, and for the stretching modes, the calculated frequencies are about 200 cm^{-1} higher than the experimental ones; this is not surprising, as anharmonicity is expected to red shift the OH stretching by about 150 cm^{-1} in isolated OH groups and even more when the latter is involved in strong hydrogen bonds, as is the case here.

I. Introduction

The study of aluminum ores is interesting from both mineralogical and commercial points of view. The major source of aluminum is bauxite, which is composed of Al oxides and hydroxides, from which Al is extracted by the Bayer process.[1]

Aluminum hydroxides exhibit the general formula (Al_2O_3,nH_2O), where n stands for the degree of hydration. Many different stable structures exist[2−4] corresponding to $n = 3$ ($Al(OH)_3$, present in four polymorphs, gibbsite, bayerite, doyleite, and nordstrandite), $n = 1$ (boehmite or γ-AlOOH and diaspore or α-AlOOH), $n = 0.25$ ($4Al_2O_3$,H_2O, akdalaite), and $n = 0.2$ ($5Al_2O_3$,H_2O, tohdite). Four of these (gibbsite, bayerite, boehmite, and diaspore) are natural solids; boehmite is the main constituent of many bauxite minerals.[5] Bayerite is not very diffuse but can easily be synthesized.[6]

The knowledge of the structure and properties of these compounds is very important because aluminum hydroxides are the hydrated precursors of transition aluminas, a family of high-surface-area oxides[7] that are widely used either as catalyst supports in refining and petrolchemical industries, in isomerization, hydrotreatment, and hydroconversion processes of residues or as sorbants for gas dehydration.[7−9] For example, when starting from boehmite, the dehydration process leads to stable α-alumina (corundum) via a great variety of metastable transition aluminas; bayerite and gibbsite give three other types of aluminas, whereas diaspore leads directly to the stable corundum phase.[2,10]

Although many experimental studies have been devoted to these systems for many years, some of their properties remain a matter of investigations.[2] The various hydroxides share several common structural properties.[2] They all consist of an oxygen network forming interstices in which Al atoms are located and octahedrally coordinated; strong hydrogen bonds are present.

In the past few years, molecular mechanics simulations[3,11] and quantum mechanical ab initio studies based on density functional theory (DFT)[1,2,7−9,12−17] have been carried out, aimed to determine the structure, the relative stability, and other properties of aluminum hydroxides. In a few cases,[8,9,12,13] the OH stretching modes are described; none of these studies, however, tackles the challenging problem of the calculation, analysis, and classification of the full vibrational spectrum and of the comparison with IR and Raman experiments.

In regards to diaspore, previous theoretical studies have been devoted to the discussion of the structure,[2,3,11,16,17] to the analysis of the relative stability with respect to other polymorphs,[2,16] and to the determination of the elastic properties and pressure effects.[14]

In the present work, we apply a quantum mechanical periodic approach based on an all-electron Gaussian-type basis set and the hybrid B3LYP Hamiltonian for the investigation of the structural and vibrational properties of diaspore. Vibrational frequencies and IR intensities at the Γ point are computed, and

* To whom correspondence should be addressed. E-mail: roberto.dovesi@unito.it.
[†] Università di Torino.
[‡] Université Pierre et Marie Curie-Paris6.
[§] Università di Torino and NIS.

10.1021/jp072501d CCC: $37.00
Published on Web 07/13/2007

a comparison with IR and Raman experiments is carried out. The latter often appear to be effected by a large uncertainty, probably due to water molecules adsorbed on the surface,[18] or loss of symmetry; broad bands as large as 800 cm^{-1} are present, and the interpretation of the spectra proposed by the various authors differs in many points. Despite that, tools implemented in the CRYSTAL code[19] (isotopic substitution, animation of the modes,[20] "freezing" part of the infinite system) permit not only a complete classification of the modes but also a one-to-one correspondence with many of the peaks proposed in the experimental papers. To the authors' knowledge, this is the first time that such a deep analysis has been carried out for one of the Al hydroxides.

The paper is organized as follows. In section II, we summarize the method employed for our calculations. The equilibrium geometry is discussed and compared to experiment in section III. Section IV is devoted to the vibrational analysis, with subsections discussing the general features of the spectrum, its OH and AlO_6 parts, and the comparison with the available IR and Raman experimental data.

II. Computational Details

The present calculations have been performed with CRYSTAL06,[19] a periodic ab initio all-electron program that uses a Gaussian-type functions (GTF) basis set.

For aluminum, the 8-621G(d) set optimized for corundum[21] has been adopted; the notation indicates that the first shell, of s type, is a contraction of 8 GTFs; there are then three sp shells, resulting from the contraction of 6, 2, and 1 GTFs. The polarization functions (of d type for Al and O, of p type for H) are indicated in parentheses; in the sp shells, the s and p functions share the same exponent. For O and H, the 8-411G-(d) and 211G(p) basis sets (18 and 6 atomic orbitals, respectively), already used in previous hydroxide calculations,[22,23] have been adopted. The exponents of the most diffuse sp and d (p for H) shells for Al, O, and H are 0.16 and 0.60, 0.17 and 0.45, and 0.14 and 1.0 $Bohr^{-2}$, respectively. Tests with larger basis sets provided essentially the same results for the properties of interest here, namely, the equilibrium geometry and the vibrational spectrum.

The B3LYP Hamiltonian has been adopted; it contains a hybrid HF/DFT exchange-correlation term. Such a Hamiltonian is widely and successfully used in molecular quantum chemistry, as well as in solid-state calculations, where it has been shown to provide excellent results for geometries and vibrational frequencies, superior to the ones obtained with LDA- or GGA-type functionals.[24−27] For the special case of the OH stretching, when not involved in hydrogen bonds,[22,23,28] B3LYP provides very accurate frequencies, once the large anharmonic effects (about 150−180 cm^{-1}) are taken into account (see below). When OH is involved in hydrogen bonds (HBs), B3LYP follows the trend of all functionals and overestimates the HB strength and red shifts the OH stretching frequencies;[29] such an overestimation is, however, less dramatic than that for other functionals due to the presence of a fraction of Hartree−Fock exchange, which underestimates the HB effects. The level of accuracy in evaluating the Coulomb and Hartree−Fock exchange series is controlled by five parameters,[19] for which the 7 7 7 7 14 values have been adopted.

The DFT exchange-correlation contribution is evaluated by numerical integration over the unit cell volume. In CRYSTAL, radial and angular points of the grid are generated through Gauss−Legendre radial quadrature and Lebedev two-dimensional angular point distributions. For the present calculations, a (75,974)*p* grid has been used (XLGRID keyword in the CRYSTAL06 manual[19]), which corresponds to a pruned grid with 75 radial and 974 angular points generating 329732 integration points in the unit cell; the accuracy in the integration can be estimated from the error in the integrated electronic charge density in the unit cell ($\Delta_e = 5.4 \cdot 10^{-5}$ $|e|$, for a total of 120 $|e|$). Frequencies are stable within 1 cm^{-1} with respect to larger grids. Further information about the grid generation and its influence on the accuracy and cost of calculation can be found in refs 24, 25, and 28.

The reciprocal space is sampled according to a regular sublattice with a shrinking factor IS equal to 8, corresponding to the choice of 125 independent **k** vectors in the irreducible Brillouin zone. The gradient with respect to the atomic and cell coordinates is evaluated analytically,[30−32] and equilibrium atomic positions are determined by using a modified conjugate gradient algorithm.[33]

In regards to the calculation of frequencies, we refer to ref 27 for a more explicit formulation of the method. Here, we simply remind one that frequencies at the Γ point have been obtained within the harmonic approximation by diagonalizing the mass-weighted Hessian matrix, **W**, whose (*i*,*j*) element is defined as

$$W_{ij} = \frac{\mathscr{H}_{ij}}{\sqrt{M_i M_j}} \tag{1}$$

where M_i and M_j are the masses of atoms associated with the *i* and *j* atomic coordinates, respectively.

Once the Hessian matrix, $\mathscr{H}$, has been calculated, frequency shifts due to isotopic substitutions can be calculated readily, at no cost, by changing masses in eq 1. In the present case, isotopic effects have been estimated by substituting ^{18}O for ^{16}O and D for H. Although the natural abundance of ^{27}Al is 100%, so that no isotopic substitution can be experimentally performed, a hypothetical isotopic substitution of ^{27}Al with ^{29}Al has been simulated as a tool for identifying the ions contributing to the modes in a given frequency range. Along the same line, sets of atoms have been assigned infinite masses so that the vibration of a fragment can be isolated without affecting the crystalline environment.

The energy first derivatives with respect to the atomic positions, $v_i = \partial V / \partial u_i$, are calculated analytically for all the u_i coordinates (*V* is the potential energy, u_i is the displacement coordinate with respect to equilibrium), whereas second derivatives at $\mathbf{u} = 0$ are calculated numerically using a single displacement along each coordinate ($N = 2$, the central point and a point on the right side of the parabola)

$$\left[\frac{\partial v_j}{\partial u_i}\right]_0 \approx \frac{v_j(0, ..., u_i, ...)}{u_i} \tag{2}$$

or averaging two displacements ($N = 3$)

$$\left[\frac{\partial v_j}{\partial u_i}\right]_0 \approx \frac{v_j(0, ..., u_i, ...) - v_j(0, ..., -u_i, ...)}{2u_i} \tag{3}$$

Both the influence of the number of points used in the evaluation of the second derivatives ($N = 2, 3$) and the magnitude of the displacements ($u = 0.001, 0.003$ Å) on the calculated frequencies have been checked for diaspore. Since the energy variations for the displacements here considered can be as small as $10^{-7}-10^{-8}$ Hartree, the tolerance on the convergence of the SCF cycles has been set to 10^{-10} Hartree.

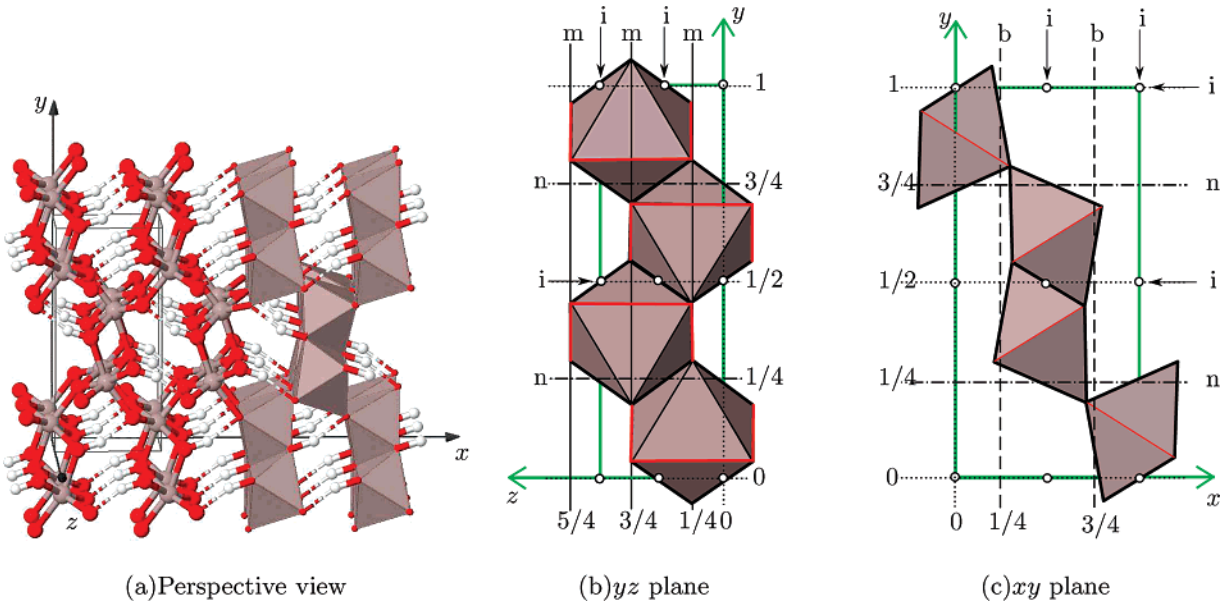

(a)Perspective view (b)yz plane (c)xy plane

Figure 1. View of the diaspore structure. On the left, a fragment of the diaspore crystal structure is presented in perspective (balls and sticks and polyhedra representations on the left and on the right in a, respectively). The four aluminum octahedra representations of the unit cell are shown projected on the *yz* (b) and *xy* (c) planes. The inversion center, mirrors, glide mirrors b, and glide mirrors n are also shown as small circles and solid, dashed, and dot-dashed lines, respectively. The unit cell and Cartesian axes are shown in green (cell vectors a, b, and c are oriented along *x*, *y*, and *z*, respectively). The rectangular equatorial plane of octahedra are underlined in red. See ref 39 for a 3D view.

TABLE 1: Comparison between Calculated Anharmonic[29,22,23,28] and Experimental OH Stretching Wavenumbers [cm^{-1}] in Systems with (β-Be(OH) $_2$,[29] Diaspore) and without Hydrogen Bonds[a]

		ω_{01}	Δ	$\omega_e x_e$	**r**(HX) [Å]
brucite − $Mg(OH)_2$	calc.	3663 3694	9 4	89.6	2.02 H
	expt.	3654 3698			−
portlandite − $Ca(OH)_2$	calc.	3637 3650	17 5	81.5	2.22 H
	expt.	3620 3645			−
edingtonite	calc.	3742	5	77.2	−
	expt.	3747			−
chabazite	calc.	3648	45	76.3	2.31 Si
	expt.	3603			−
katoite − $Al_2Ca_3(OH)_{12}$	calc.	3673	12	86	1.93 H
	expt.	3661			−
β-$Be(OH)_2$	calc.	3326 3269	138 171	122 134	2.18 2.15
	expt.	3464 3440			2.01 1.99
diaspore − α-AlOOH	calc.	2731	190	215.6	1.69
	expt.	2920			1.68

[a] Edingtonite[28] can be used as a model for surface OH groups in silica; chabazite[28] is an acid zeolite; **r**(HX) is the distance of H from the nearest atom, which is indicated on the right (as edingtonite consists of surface OH Groups, no neighbor is indicated for H); for the last two systems, where HB is present, **r**(HX) gives the distance from the nearest oxygen atom. Δ is the absolute difference between calculated and experimental values. Note that OH stretching frequencies of non-HB systems agree very well with experiment and that the anharmonic constant is in the range of 75−90 cm^{-1}. When HB is present, as in β-$Be(OH)_2$ and α-AlOOH, its strength is overestimated; in particular, the shorter the HB, the larger the overestimation: the anharmonic constants become very large, and Δ increases dramatically.

The variability of the calculated frequencies, ν_{calc}, as depending on a general parameter (in this case N and u), is estimated through two global indices evaluated with respect to a reference set of M frequencies, ν^{ref}_{calc}, as follows

$$|\bar{\Delta}| = M^{-1} \sum_{calc=1}^{M} |\nu_{calc} - \nu^{ref}_{calc}|$$

$$\Delta_{max} = \max|(\nu_{calc} - \nu^{ref}_{calc})| \qquad (4)$$

Regarding N, $|\bar{\Delta}|$ is 0.6 cm^{-1} and Δ_{max} = 6.8 cm^{-1}, with ν^{ref}_{calc} being ν values calculated with $N = 3$ and ν_{calc} the ones calculated with $N = 2$. A larger dependence of OH harmonic stretching frequencies on u has been found, with $|\bar{\Delta}| = 1.5$ cm^{-1} and $\Delta_{max} = 10.3$ cm^{-1}.

Previous calculations[24,25,27] have shown that the influence of both u and N is very small (less than 1 cm^{-1}) when H atoms are not present; much larger effects are found for katoite[23] and brucite.[22] Such a large effect is mainly related to the anharmonicity of the OH stretching. Anharmonicity increases dramatically when hydrogen-bonded systems[28,29] are considered (see Table 1), and we will see later on that diaspore belongs to this latter family.

For this reason, we try to estimate the anharmonicity of the OH stretching modes as follows. The one-dimensional Schrödinger equation for the anharmonic OH oscillator has been solved numerically, starting from total energies evaluated for various O−H distances. This scheme produces the first three eigenvalues, which can be used to estimate the anharmonic constant $\omega_e x_e$ and the approximated harmonic frequency ω_e as follows

$$\omega_{01} = E_1 - E_0$$

$$\omega_{02} = E_2 - E_0$$

$$\omega_e x_e = \frac{(2\omega_{01} - \omega_{02})}{2}$$

$$\omega_e = \omega_{01} + 2\omega_e x_e \qquad (5)$$

The IR intensity of the ith mode is defined as

$$A_i \propto d_i \left| \frac{\partial \mu}{\partial Q_i} \right|^2 \qquad (6)$$

that is, they are proportional to the square of the first derivative of the dipole moment with respect to the normal coordinate Q_i (evaluated through well-localized Wannier functions[34−37]) times the d_i degeneracy of the ith mode.

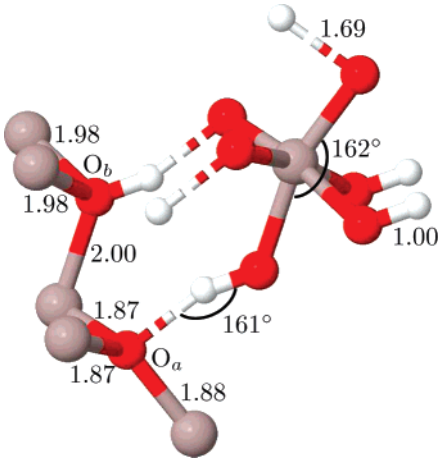

Figure 2. Representation of a diaspore fragment. Aluminum, oxygen, and hydrogen are represented in gray, red, and white, respectively. The Al octahedron is shown on the right, and the O_a and O_b fourfold coordination are on the left. The distance of oxygen atoms from the plane of the three aluminum atoms is 0.35 and 1.07 Å for O_a and O_b, respectively. Dotted lines indicate hydrogen bonds (HBs); O_b and O_a atoms are HB donors and acceptors, respectively. Distances are in angstroms, and angles are in degrees. See ref 39 for a 3D view.

Manipulation and visualization of structures have been performed with the MOLDRAW program.[38] The web page[39] presenting the diaspore vibrational modes has been performed by using the Jmol[40] 3D engine and created by using the WEBVIB[41] script.

III. Structure

The diaspore crystal belongs to the orthorhombic *Pbnm* space group (group number 62, or D_{2h}^{16}; there are 8 symmetry operators, namely, E, $2_1(x)$, $2_1(y)$, $2_1(z)$, i, $b(yz)$, $n(xz)$, and $m(xy)$). Its structure (see Figure 1 or ref 39 for a 3D view) is defined by four irreducible atoms (Al, O_a, O_b, and H), lying on the xy plane at $z/c = 1/4$ (m site symmetry with fourfold multiplicity; see Figure 1b). The unit cell contains then 16 atoms (four symmetry-equivalent AlOOH units). The aluminum atom is surrounded by six oxygen atoms, forming an irregular octahedron (see Figure 1a). The Al and both axial O atoms (one O_a and one O_b) lie on a mirror plane so that the four equatorial oxygen atoms (two O_a and two O_b) form a rectangle (Al is slightly off-center). The AlO_a axial vector is almost perpendicular to the equatorial plane, whereas the other half of the octahedral axis (AlO_b) is bent by about 18° ($\angle$OAlO is then equal to 162°; see Figure 2). O_a and O_b are tetrahedrally coordinated, as shown in Figure 2 (in 3D in ref 39). Three of the neighbors are Al atoms at about 1.88 (O_a) and 1.98 Å (O_b) (data refer to the calculated geometry). The fourth link is to a H atom, directly bonded for O_b (at 1.00 Å) or hydrogen bonded for O_a (at 1.69 Å); see Figure 2. Then, all O atoms are involved in hydrogen bonds as donors (O_b, directly linked to H) or acceptors (O_a).

The AlO_6 octahedra are linked together to form chains in the z direction[42] by edge-sharing ensured by two equatorial oxygen atoms (one O_a and one O_b). Two parallel z chains are connected through two O_b atoms, each O_b being axial in an octahedron and equatorial in the other (see Figure 1b). These double chains (whose octahedra have the same orientation) are joined to similar ones (but with a different orientation) by sharing an O_a atom (O_a is axial in a chain and equatorial in the other). Oxygen atoms are shared between three octahedra. The stacking of octahedra double chains creates large tunnels along z, as shown in Figure 1a; hydrogen atoms divide this empty space into one large and two small cavities.

TABLE 2: Comparison between Calculated and Experimental[43] Diaspore Structural Data (ax = Axial, eq = Equatorial); Δ Is the Absolute Difference[a]

	calc.	expt.[43]	Δ
a	4.433	4.401	0.032
b	9.484	9.425	0.059
c	2.870	2.845	0.025
$(Al-O_a)_{eq}$	1.881	1.867	0.014
$(Al-O_a)_{ax}$	1.867	1.852	0.015
$(Al-O_b)_{eq}$	1.981	1.966	0.015
$(Al-O_b)_{ax}$	1.999	1.985	0.014
O_b-H	0.996	0.989	0.007
$O_a\cdots H$	1.687	1.676	0.011
$O\widehat{H}O$	161.2	160.7	0.5

[a] Distances in angstroms, and angles in degrees.

The calculated and experimental[43] structures are shown in Table 2; they are in excellent agreement. For example, differences in Al−O and O−H distances are smaller than 0.02 and 0.01 Å, respectively.

The Mulliken analysis provides a schematic (and, in part, arbitrary) description of the charge distribution in the unit cell in terms of charge and bond terms; in the present case, net charges are +2, −1.33, −1.12, and +0.45 $|e|$ for Al, O_a, O_b, and H, respectively, and overlap populations are +0.102 ($Al-O_a$), +0.045 ($Al-O_b$), and +0.257 (O_b-H) $|e|$. In order to put these numbers on a comparative scale, the equivalent data for fully ionic and quite covalent compounds such as MgO and α-quartz are +1.52 (Mg), 0.05 (Mg−O), +1.58 (Si), and +0.30 (Si−O) $|e|$. As expected, these numbers confirm the semi-ionic character of the Al−O bonds (in particular, $Al-O_b$) and the strong covalent character of O_b-H.

IV. Frequency Analysis

Decomposition of the reducible representation built on the basis of the Cartesian coordinates of the unit cell atoms leads to the following symmetry assignment of the 48 normal modes

$$\Gamma_{total} = 4B_{1u} + 8B_{2u} + 8B_{3u} + 8B_{1g} + 4B_{2g} + 4B_{3g} + 4A_u + 8A_g \quad (7)$$

There are then 20 IR ($3\ B_{1u} + 7\ B_{2u} + 7\ B_{3u}$), 24 Raman ($8\ B_{1g} + 4\ B_{2g} + 4\ B_{3g} + 8A_g$) and 4 "silent" A_u modes; the lowest frequencies of B_{1u}, B_{2u}, and B_{3u} symmetry, corresponding to pure translations, are null.

As all atoms are in an m site position (see section III), eigenvectors can be split into two groups (see the D_{2h} characters table): (a) eigenvectors symmetric with respect to m (A_g, B_{1g}, B_{2u}, and B_{3u}); this corresponds to movements in the xy plane and will be referred as D_{xy}; and (b) eigenvectors antisymmetric with respect to m (A_u, B_{1u}, B_{2g}, and B_{3g}); this corresponds to movement orthogonal to the xy plane, which is along z and will be referred as D_z. This factorization simplifies the graphical representation of modes.

A hypothetical isolated AlOOH unit (4 atoms) would generate 12 normal modes. Through the interaction with the other three AlOOH units of the diaspore unit cell, each one of the 12 modes generates a set of 4 modes (the "band of the set"). Within each set, modes have roughly the same atomic coefficients for the AlOOH unit. AlOOH units, however, combine with different phases to give the four vectors of the set. At high frequency (in the hydrogen region; see further on in this section), modes are well separated, and the movement of the four equivalent units

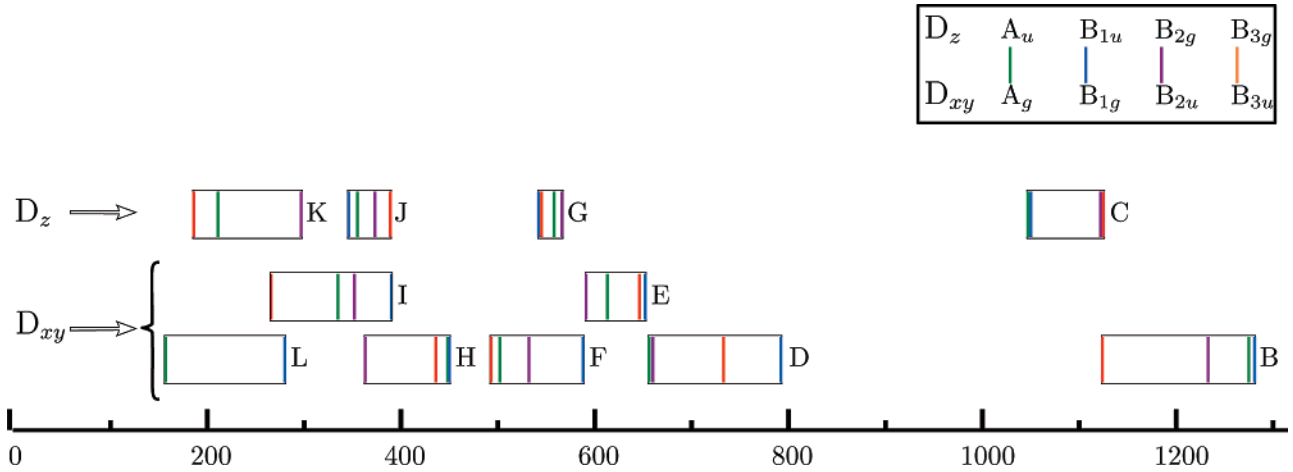

Figure 3. Schematic view of diaspore modes as sets of four. The horizontal axis indicates frequencies in cm^{-1}. Each mode is represented by a vertical line whose color indicates its symmetry (see key at the top-right corner). Sets of four modes are included in a rectangle for a better identification. The two different types of sets (D_z and D_{xy}) are separated vertically, the former (modes with A_u, B_{1u}, B_{2g}, and B_{3g} symmetry) in the high part of the figure and the latter (A_g, B_{1g}, B_{2u}, and B_{3u} symmetry) in the lowest part of the figure. D_{xy} sets are reported in two different rows in order to evidence the overlap among the sets. The three lowest modes (B_{1u}, B_{2u}, and B_{3u}) correspond to translations and are not reported. Sets are labeled from A to L (on the right of the set). Set A (OH stretching at about 31501 cm^{-1}) is not shown. See text for details.

TABLE 3: O_b−H and H···O_a Distances (Å) and OH Harmonic Stretching Frequency ν (cm^{-1}) of Diaspore Obtained with Different Hamiltonians; the B3LYP OH Distances Are Close to Experiment, and So Is for the OH Frequency, whereas PBE and LDA Overestimate the OH Bond Length and Give Very Low Frequencies

	expt.[43,45]	B3LYP	PBE	LDA
O−H	0.9891	0.9962	1.0255	1.0656
HB	1.6757	1.6874	1.5882	1.4370
ν	2900,3000	3137−3166	2702−2735	2230−2275

is only loosely correlated so that the bands of the sets are narrow and well separated from each other (see Figure 3). In the low region of the spectrum (octahedra modes; see further on in this section), on the contrary, frequencies are closer and the bands of the sets are broad and overlap with each other. Since it is difficult here to attribute a mode to one set or another without ambiguity, sets are identified on the basis of the pure sequential order of the four symmetries characterizing the set, A_g, B_{1g}, B_{2u}, and B_{3u} for the D_{xy} sets and A_u, B_{1u}, B_{2g}, and B_{3g} for the D_z sets, as shown in Figure 3. The 3D animation[39] shows that, within a set, displacements of AlOOH units are quite different, indicating a strong mixing between sets.

The diaspore spectrum, whose frequencies are given in Table 4, can be divided into three regions, separated by large gaps, (1) the 150−800 cm^{-1} region, where the Al−O octahedron modes are active, (2) the 1050−1300 cm^{-1} zone, containing Al−OH "in-plane" (that is, bending modes modifying the AlOH angle) and "out-of-plane" (or "rotations"; H rotates around the Al−O axis, keeping the AlOH angle nearly constant) bending modes, and (3) the OH stretching region, at about 3150 cm^{-1}.

Such a schematic partition is supported by various complementary tools that have been used for analyzing the nature of the modes, (1) isotopic substitution, (2) decomposition of the spectrum into subunits, and (3) animations.[20]

TABLE 4: Diaspore Vibrational Modes and Effect of the ^{29}Al, $^{18}O_a$,$^{18}O_b$, and D Isotopic Substitutions on the Calculated Wavenumbers ν (cm^{-1}); Isotopic Shifts Larger than 2 cm^{-1} Are in Bold Type

	sym	ν	$\Delta\nu$ with isotopic substitutions					sym	ν	$\Delta\nu$ with isotopic substitutions			
			^{29}Al	$^{18}O_a$	$^{18}O_b$	D				^{29}Al	$^{18}O_a$	$^{18}O_b$	D
1	A_g	159.1	**2.7**	4.1	1.0	1.2	24	B_{2g}	567.6	**4.6**	**22.3**	1.5	**4.6**
2	B_{3g}	188.8	**4.1**	**4.3**	0.2	0.2	25	B_{1g}	590.1	**5.4**	**12.7**	**13.8**	**13.1**
3	A_u	213.8	**3.3**	1.0	**6.4**	**3.0**	26	B_{2u}	592.0	**9.3**	**5.7**	**14.1**	**14.0**
4	B_{3u}	267.7	**3.9**	1.2	**8.2**	**4.5**	27	A_g	614.6	**7.2**	**11.2**	**17.2**	**9.9**
5	B_{1g}	281.9	**5.3**	**6.8**	1.6	0.6	28	B_{3u}	647.6	**13.5**	1.6	**13.1**	**6.2**
6	B_{2g}	299.2	**8.2**	**4.2**	0.2	0.5	29	B_{1g}	653.7	1.7	**10.4**	**18.7**	**13.1**
7	A_g	337.4	**3.7**	**8.9**	**5.7**	0.8	30	B_{2u}	658.1	1.2	**23.9**	**7.5**	1.2
8	B_{1u}	347.5	**2.1**	**2.6**	**13.8**	**3.7**	31	A_g	661.6	1.4	**17.0**	**8.9**	**14.7**
9	B_{2u}	354.4	**4.5**	**14.2**	**3.1**	**5.2**	32	B_{3u}	734.5	0.7	**32.5**	**6.8**	1.1
10	A_u	357.1	**4.4**	**4.1**	**9.3**	1.4	33	B_{1g}	793.9	**8.6**	**28.3**	0.7	**16.1**
11	B_{2u}	364.5	**3.8**	0.8	**10.9**	**2.4**	34	A_u	1047.9	0.0	0.6	**2.1**	**284.8**
12	B_{2g}	374.8	0.0	1.6	**19.9**	**2.4**	35	B_{1u}	1049.4	0.0	0.3	**2.1**	**288.7**
13	B_{3g}	391.2	0.1	0.7	**21.5**	**3.4**	36	B_{2g}	1124.5	0.0	0.5	1.2	**313.1**
14	B_{1g}	392.3	**5.5**	**5.0**	**10.7**	**7.6**	37	B_{3u}	1125.7	0.1	1.3	**3.6**	**288.5**
15	B_{3u}	437.7	**7.9**	**6.8**	**7.9**	1.5	38	B_{3g}	1126.4	0.0	0.3	1.1	**316.2**
16	A_g	449.9	**10.5**	1.9	**8.5**	**3.6**	39	B_{2u}	1235.2	1.9	1.6	**6.0**	**282.2**
17	B_{1g}	452.1	**7.1**	**2.3**	**10.8**	**4.0**	40	A_g	1277.0	0.7	1.4	**3.4**	**325.0**
18	B_{3u}	495.2	0.2	**15.9**	**8.0**	**16.8**	41	B_{1g}	1282.7	0.6	2.0	**3.8**	**315.2**
19	A_g	504.4	**2.9**	**7.7**	**13.5**	**13.3**	42	A_g	3137.2	0.1	0.1	**11.8**	**833.5**
20	B_{2u}	533.7	**6.9**	**5.7**	**9.9**	**29.8**	43	B_{1g}	3155.3	0.1	0.0	**11.5**	**840.1**
21	B_{1u}	544.2	**7.3**	**18.7**	0.0	1.2	44	B_{3u}	3159.0	0.1	0.1	**9.6**	**853.6**
22	B_{3g}	547.1	**7.5**	**18.4**	0.2	1.8	45	B_{2u}	3165.5	0.1	0.1	**10.5**	**851.0**
23	A_u	560.3	**4.7**	**23.2**	0.3	4.1							

TABLE 5: Shift of the "Hydrogen" Frequencies ν (cm^{-1}) Obtained by Attributing Infinite Masses (a Progressive "Freezing" of the System) to the Al, AlO_a, and AlO_aO_b Groups[a]

	sym	ν	$\Delta\nu$ with isotopic substitutions		
			Al	AlO_a	AlO_aO_b
34	A_u	1047.9	0.0	**4.0**	**21.6**
35	B_{1u}	1049.4	0.0	1.8	**19.4**
36	B_{2g}	1124.5	0.0	**3.7**	**12.6**
37	B_{3u}	1125.7	1.1	**9.8**	**39.7**
38	B_{3g}	1126.4	0.1	2.0	**11.1**
39	B_{2u}	1235.2	**23.7**	**35.1**	**81.9**
40	A_g	1277.0	**9.5**	**20.0**	**47.5**
41	B_{1g}	1282.7	**7.1**	**18.3**	**50.2**
42	A_g	3137.2	1.4	**2.2**	**106.0**
43	B_{1g}	3155.3	1.8	**2.4**	**103.8**
44	B_{3u}	3159.0	**2.3**	**3.0**	**89.0**
45	B_{2u}	3165.5	1.6	**2.5**	**95.6**

[a] Frequencies of modes 1−33 are shifted by hundreds of wavenumbers also when Al only is substituted.

A. The OH Modes. The light mass of hydrogen is responsible for the separation from the rest of the spectrum of the 12 "hydrogen" modes due to the presence of 4 interacting OH groups, leading to 4 stretching, 4 in-plane, and 4 out-of-plane bending modes. Table 4, showing the effect of the isotopic substitution on the full set of frequencies, confirms that when H atoms are replaced by deuterium, the 12 "hydrogen" modes are shifted by 250−350 cm^{-1} (bending modes) or by as much as 800 cm^{-1} (stretching modes). Note that the largest shift due to deuterium for all other modes is only 30 cm^{-1}, confirming the totally different nature of the 12 highest modes.

The effect of the substitution $^{16}O \rightarrow {}^{18}O$ for the oxygen atoms bonded to H (O_b) is obviously much smaller because of the smaller relative mass variation; it is, however, interesting to notice that it is quite different for the three kind of modes, about 10 cm^{-1} for stretching modes (O_b moves forward and backward in order to keep the center of mass unaltered), 3−6 cm^{-1} for in-plane bending modes, and only 1−2 cm^{-1} for out-of-plane bending modes (where O is essentially not involved). The isotopic substitutions of aluminum and O_a do not influence these modes significantly (the largest shift being 2 cm^{-1}).

A further evidence that the 12 highest modes are dominated by H atom displacements is obtained by "freezing" all atoms but H. Computationally, this is obtained by attributing infinite (in practice, extremely large) masses to Al, O_a, and O_b in the mass-weighted Hessian matrix (see eq 1). In this way, only hydrogen atoms are allowed to move; as a consequence, the frequencies of the modes to which Al, O_a, and O_b give important contributions will shift down a lot. On the contrary, the frequencies of nearly pure hydrogen modes will shift moderately.

It turns out (see Table 5) that stretching modes (at about 3150 cm^{-1}) shift by about 100 cm^{-1}; the shift Δ is even smaller for the in-plane bending modes (50 cm^{-1}) due to the smaller participation of O_b and nearly negligible for the out-of-plane bending modes (only 15 cm^{-1}), confirming that the latter are essentially pure "hydrogen" modes.

The stretching band is quite narrow (about 30 cm^{-1}; set A is not represented in Figure 3), as the interaction between AlOOH units is weak. The set B corresponds to in-plane (D_{xy}) bending modes and is 157 cm^{-1} wide. In two of the modes (A_g and B_{1g}), H atoms move in the cavities in antiphase so that the H−H distance at one extreme of the motion is much smaller than that at equilibrium; this produces a shift toward high frequencies. In the other two modes (B_{2u} and B_{3u}), H atoms move in-phase so that the H−H distance remains nearly constant. The second bending band (set C in Figure 3) is 80 cm^{-1} wide. Also, this set (D_z type) splits in two subsets, the first (A_u and B_{1u} modes) at lower frequencies because the H movements keep the H−H distance nearly constant and the second (B_{2g} and B_{3g} modes) blue shifted by 75 cm^{-1}, in which the H−H distance is not constant along the vibration coordinates (see also the 3D animation[20]).

As anticipated in section II, OH stretching frequencies are strongly effected by anharmonicity. Due to the nearly pure nature of the OH stretching (in particular, when not involved in hydrogen bonds), anharmonicity can be estimated by computing the total energy of the system for various O−H distances and then by numerically solving the one-dimensional Schrödinger equation for the anharmonic oscillator.

The resulting anharmonic correction is, in this case, extremely large ($2\omega_e x_e = 430$ cm^{-1}), certainly much larger than it should be. There are two main reasons for this overestimation. (a) One is related to the adopted Hamiltonian;[48] B3LYP provides OH equilibrium distances longer than the experimental ones, in particular, when HBs are present. This feature is common to all DFT-based approaches and is much more dramatic for LDA or GGA than that for B3LYP (see Table 3). (b) The second is due to the fact that, when H is involved in HBs, the H atom is no longer the terminal of a chain pointing toward vacuum or cavities; the independent motion of H along the $O_b-H\cdots O_a$ direction brings H very close to O_a. In a coupled motion, on the contrary, the OH stretching and the $O_b\hat{H}O_a$ bending modes increase both the $H-O_a$ distance and the $O_b-H\cdots O_a$ angle, reducing then the HB interaction. In addition, as the HB distance is very short, the O_b-H and $O_a\cdots H$ stretching modes are expected to couple, and therefore, the independent mode model fails. As a consequence the "true" anaharmonic frequency is somewhere in between the harmonic frequency and the anharmonic one estimated on the basis of the independent motion. As when there are no HBs, the anharmonicity of the OH stretching has been estimated at about 150−180 cm^{-1}.[22,23,28] We can guess that, in the present case, it should be overestimated by about 150−200 cm^{-1}; that means that the term $2\omega_e x_e$ would fall in the range 220−270 cm^{-1}. The obtained values, then, must be considered as upper limits for anharmonicity.

B. The AlO_6 Modes. There are 33 octahedra modes lying in the 150−800 cm^{-1} region, divided into 3 D_z and 6 D_{xy} sets (labeled from D to L in Figure 3). One set of each type is incomplete due to translations.

The classification of the isolated octahedron modes[44] might be used, in principle, as a guideline in our analysis. We do not find, however, a direct correspondence between the "perfect-isolated octahedron" modes and our "real" solid system. For this reason, it is difficult to classify the various sets of frequencies shown in Figure 3 into simple categories. Animation[20] is, however, a useful and powerful tool for the classification of modes, as it provides direct evidence of the involved atoms.

Let us consider first the D_{xy} sets, each of which involves four modes of A_g, B_{1g}, B_{3u}, and B_{2u} symmetry. Modes in sets D and E in Figure 3 mainly represent the $Al-O_a$ and $Al-O_b$ stretching modes, respectively. Modes in sets F and H correspond mostly to bending motions and to the stretching of the axial O−Al−O bonds. The two last sets (I and L), in the lowest part of the spectrum, correspond to rotation/bending movements of the octahedra. With regards to the D_z sets, they include modes having A_g, B_{1g}, B_{3u}, and B_{2u} symmetry. Sets G and J are found to correspond to octahedra bending modes, whereas the lowest D_z set (K) corresponds to rotation/translation of the octahedra.

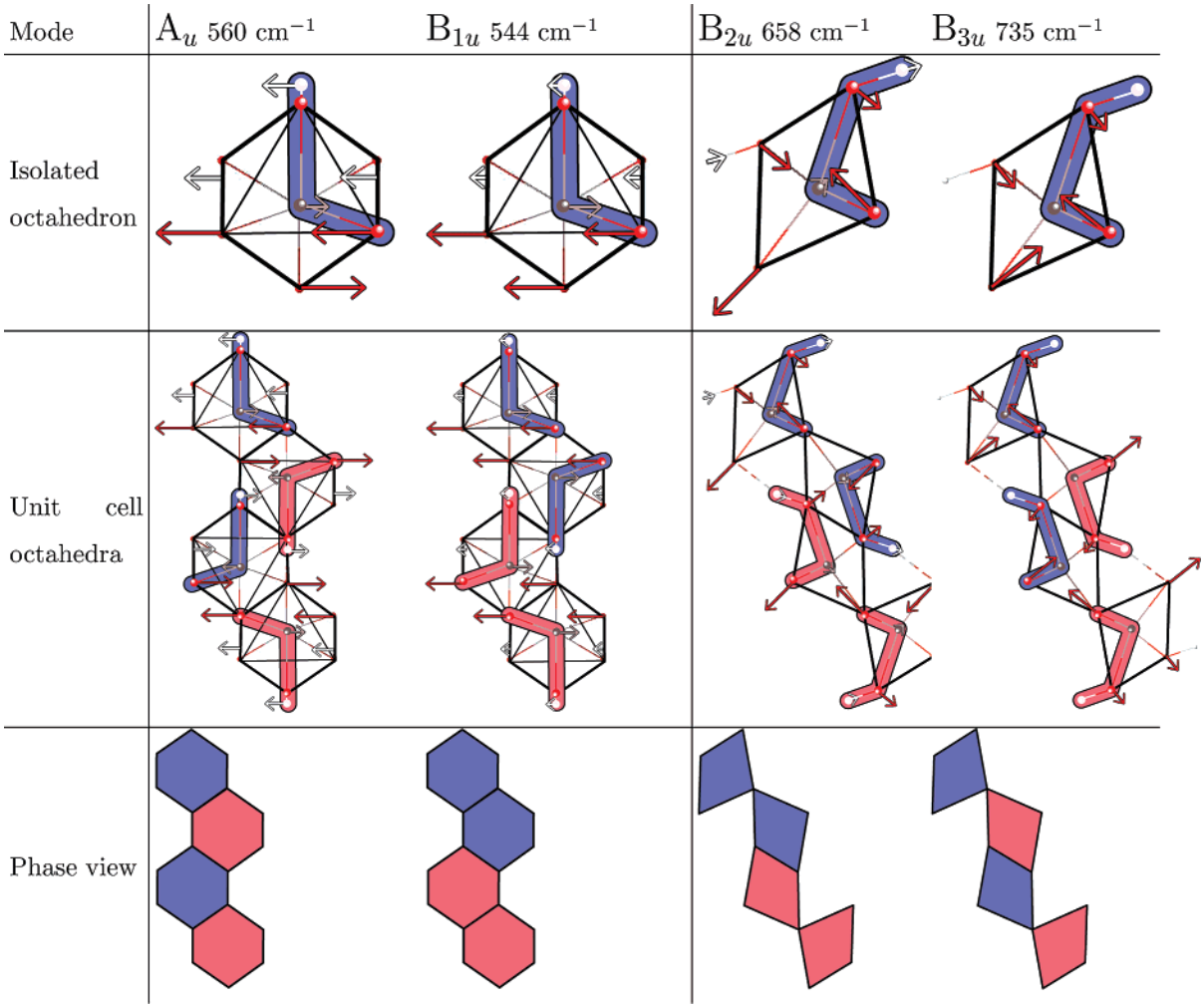

Figure 4. Analysis of vibrational modes of diaspore. Four eigenvectors, two of a D_z (left) and two of a D_{xy} (right) set, have been considered as examples for illustrating the various symmetry combinations. In the top figures, one of the four octahedra (the top one) of the unit cell is shown. Arrows are proportional to the atomic displacements (small coefficients have been neglected). The AlOOH unit is evidenced in blue. In the middle figure, the four independent octahedra contained in the unit cell are represented. The same (different) color underlines the in-phase (antiphase) movement. In the bottom figure, the phase or antiphase classification of the AlOOH groups on the basis of color is attributed to the full octahedron. Note that within a set (D_z or D_{xy}), atomic displacements of a single AlOOH unit are similar, whereas octahedra deformations are different due to the different phase combinations of the four AlOOH units. The same colors as those in Figure 2 have been used for atoms.

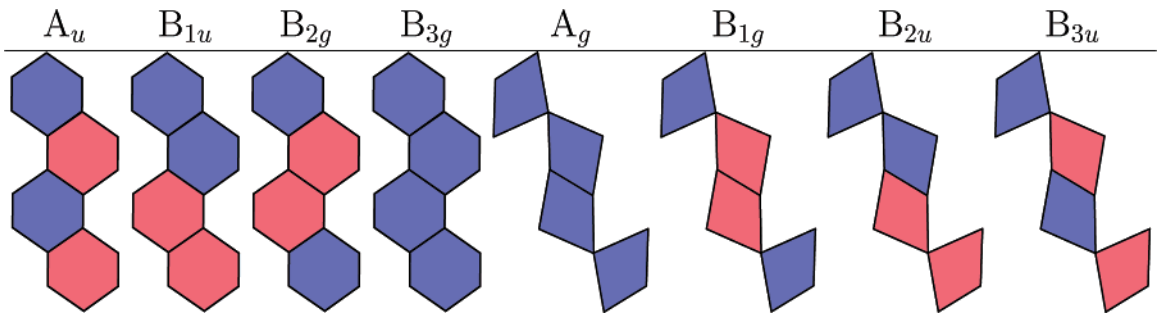

Figure 5. Schematic representation of the behavior of each octahedron for the eight possible symmetries. Unit cell octahedra are represented as in Figure 1b and c. As in Figure 4, the same color is used for octahedra moving in phase (different colors corresponding to antiphase movements).

In Figure 4, two modes of a D_z set and two of a D_{xy} set are sketched as examples of the above analysis. Atomic displacements are represented with arrows proportional to the atomic coefficients in the eigenvectors. AlOOH units are in blue or red, according to their in-phase or antiphase movement. The top figure shows a single octahedron (note that within a set, the displacements in a single octahedron are the same), whereas the middle figure shows how the four independent octahedra of the unit cell combine to give the various modes of the set. This analysis is even clearer in the bottom figure, where the color is attributed to the full octahedron. In Figure 5, the same scheme is applied to the analysis of the phase combinations of the four independent octahedra of the unit cell for the eight symmetries.

C. Comparison with Experimental IR and Raman Data. We have been able to find four IR[6,42,44,45] and two Raman[18,46] experimental sets of vibrational data referring to pure diaspore. A few other IR spectroscopic studies[10,47] are available, which,

TABLE 6: Calculated and Experimental IR Frequencies of Diaspore[a]

	sym	ν_{calc}	A	Stegmann[45]	Frost[42]	Farmer[44]	Ruan[6]
1		–	–	–	–	–	199 187 159
2	B_{3u}	267.7	2	–	–	–	250 237
3		–	–	305 sh.	–	–	–
4	B_{1u}	347.5	460	–	–	–	331
5	B_{2u}	354.4	440	350	–	–	354
6	B_{2u}	364.5	150	372	–	–	373
7		–	–	–	–	–	394
8	B_{3u}	437.7	2400	–	–	–	
9	B_{3u}	495.2	20	489 sh.	–	–	–
10	B_{2u}	533.7	300	520	–	–	–
11	B_{1u}	544.2	2000	–	–	–	–
12	B_{2u}	592.0	1300	572	–	–	–
13	B_{3u}	647.6	20	640 sh.	–	–	–
14	B_{2u}	658.1	400	670	–	–	–
15	B_{3u}	734.5	200	750	–	–	–
16		–	–	960	–	963	–
17	B_{1u}	1049.4	1000	1086 (B_{1u})	1079	1077	–
18	B_{3u}	1125.7	1300	1155 sh. (B_{3u})	1151	–	–
19	B_{2u}	1235.2	10	–	–	–	–
20		–	–	2110 1985	–	2000 2100	–
21 h	B_{3u}	3159.0	1400	2910 (B_{3u})	2938	2915	–
21 a		2727.8	–				–
22 h	B_{2u}	3165.5	6100	2995(B_{2u})	3095	2994	–
22 a		2734.3	–				–
23		–	–	–	3365 3284	–	–

[a] The ν are the IR wavenumbers, in cm^{-1}; *A* is the calculated intensity in km/mol; sh. stands for shoulder. Breaks in the table are used to divide the three spectrum zones, the octahedra modes, the Al−OH bending modes, and the OH stretching modes; experimental symmetry labels, when available,[45] are indicated in parentheses. Both the calculated harmonic h and anharmonic a stretching frequencies are given for OH.

TABLE 7: Calculated and Experimental Raman Wavenumbers (cm^{-1}) of Diaspore[a]

	sym	ν_{calc}	Ruan[18]	RASMIN[46]		sym	ν_{calc}	Ruan[18]	RASMIN[46]
1	A_g	159.1	–	–	17	A_g	661.6	664	**662**
2	B_{3g}	188.8	*207* 216	–	18		–	**705**	–
3	B_{1g}	281.9	*287* **260**	–	19	B_{1g}	793.9	790	*782*
4	B_{2g}	299.2	–	–	20		–	*812 837 918 956*	–
5	A_g	337.4	329	**328**	21		–	*1018 1045 1067*	–
6	B_{2g}	374.8	*364* 381	–					
7	B_{3g}	391.2	–	–	22	B_{2g}	1124.5	–	–
8	B_{1g}	392.3	*394*	–	23	B_{3g}	1126.4	–	–
9	A_g	449.9	436 **446**	**446**	24		–	*1186*	*1180*
10	B_{1g}	452.1	466	–	25	A_g	1277.0	–	–
11	A_g	504.4	*495*	*488*	26	B_{1g}	1282.7	–	–
12	B_{3g}	547.1	*552*	545					
13	B_{2g}	567.6	–	–	27 h	A_g	3137.2	2936	–
14	B_{1g}	590.1	*580*	–	27 a		2706.0		
15	A_g	614.6	609	*603*	28 h	B_{1g}	3155.3	3119	–
16	B_{1g}	653.7	–	–	28 a		2724.1		

[a] Bold and italic numbers refer to very intense and weak peaks in the experimental spectrum, respectively. The RASMIN[46] database provides data in the 200−1400 cm^{-1} interval only. Solid lines separate the octahedral, Al−OH bending, and OH stretching zones. The h stands for harmonic, and a is for anharmonic.

however, refer to samples containing impurities that strongly influence the vibrational spectrum so that a direct comparison with the present calculated data is not possible.

As anticipated, there are 17 IR active modes (see Table 6), 12 involving mainly the Al−O octahedra ($2B_{1u} + 5B_{2u} + 5B_{3u}$) and 5 the OH groups ($B_{1u} + 2B_{2u} + 2B_{3u}$), and 24 Raman active modes (see Table 7), 18 for the Al−O octahedra ($6A_g + 6B_{1g} + 3B_{2g} + 3B_{3g}$) and 6 for the OH groups ($2A_g + 2B_{1g} + B_{2g} + B_{3g}$).

Calculated and observed[6,42,44,45] IR peaks are given in Table 6. In the experimental papers, peaks are symmetry-classified only in few cases; their nature is scarcely discussed (or not at all), and the individual intensities are not reported. The spectrum appears dominated by very broad bands, as large as 800 cm^{-1} in the OH stretching zone; individual peaks within these bands are obtained by the band component analysis, corresponding to a best fit of the spectrum with a Lorentz−Gauss cross-product function (for example, the Raman OH stretching band is fitted by a function with five bands[18]). In these conditions, the one-to-one correspondence between calculated and observed peaks can be performed only on the basis of frequency similarity.

The most complete set of IR data, provided by Stegmann et al.,[45] shows 6 clear bands (at 350, 372, 520, 572, 670, and 750 cm^{-1}) and 3 shoulders (at 305, 489, and 640 cm^{-1}) in the Al−O octahedral zone (150−800 cm^{-1}), where calculation provides 12 peaks. Eight of these nine experimental peaks do have a calculated counterpart, with wavenumber differences never larger than 20 cm^{-1} (mean absolute difference $|\bar{\Delta}| = 10.9$ cm^{-1}); the experimental shoulder at 305 cm^{-1}, on the contrary, does

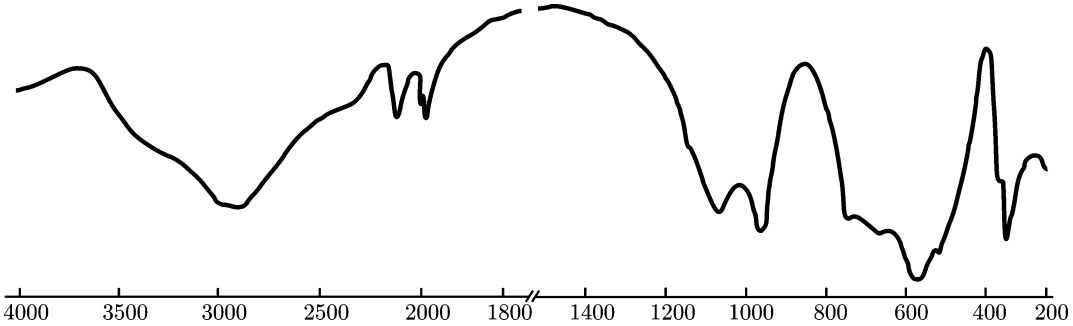

Figure 6. Absorption experimental IR spectrum of diaspore monocrystal sheets. Reprinted from[45] Stegmann, M. C.; Vivien, D.; Mazieres, C. Etude des modes de vibration infrarouge dans les oxyhydroxides d'aluminum boehmite et diaspore. *Spectrochim. Acta, Part A* **1973**, *29*, 1656 (Figure 2) and 1661 (Figure 6), with permission from Elsevier. Copyright 1973.

not appear in our IR calculated list (the nearest peak is 40 cm^{-1} away) nor in the low-frequency determination by Ruan et al.[6]

Why are four calculated peaks not observed in Stegmann's experiment? For three of them, the explanation is simple; the intensity of the peak at 267 cm^{-1} is extremely low, and the very close calculated peaks at 347 and 354 and at 533 and 544 cm^{-1} are probably seen as a single band (centered at 350 and 520 cm^{-1}) in the experiment. The very intense calculated peak at 437 is not seen in the experiment; the two closest calculated peaks at 364 and 495 cm^{-1} (then 60 cm^{-1} away) do have, on the contrary, corresponding experimental peaks nearby (at 372 and 489). We must then suppose that in the component analysis of the broad band dominating this part of the spectrum, this large peak has been missed; as shown in Figure 6, in fact, a single notched band as large as 350 cm^{-1} is present in the region of 400−800 cm^{-1}. Stegmann's spectrum[45] shows also a peak at 960 cm^{-1}; this peak, as well as those reported in the 1900−2300 cm^{-1} region by various authors,[10,44,45] certainly corresponds to overtones or combinations, as they are very far from any calculated peak.

The far-IR experiment, carried out by Ruan et al.,[6] gives a spectrum in the 180−400 cm^{-1} range richer than the calculated one in the corresponding zone; four peaks are in good agreement with ours (373 vs 364.5, 354 vs 354.4, 331 vs 347.5, and 250 vs 267.7 cm^{-1}). Ruan's extra modes at 237 cm^{-1} derive from a band component analysis of a relatively large band with a small shoulder. Three other peaks have been observed by Ruan at 394, 187, and 159 cm^{-1}, which do not have any calculated counterpart; it turns out, however, that they are very close to four of our Raman peaks (391.2, 392.3, 188.8, and 159.1 cm^{-1}). Finally the observed peak at 199 cm^{-1} (see Table 6) is close to our calculated frequency at 213 cm^{-1}; that is, however, a silent mode. A possible reason for these unexpected experimental peaks is a symmetry loss (due to defects or disorder) that might transform silent or Raman active modes into IR active modes.

Differences between experiment and simulation are larger in the OH part of the spectrum. Peaks at 1086 and 1155 cm^{-1} have been interpreted as bending and rotation modes by Stegmann[45] and symmetry-classified as B_{1u} (rotation) and B_{3u} (bending), respectively. The calculated frequencies for these modes confirm the symmetry attribution but are 37 and 30 cm^{-1} lower, respectively. Values close to Stegmann's[45] have been obtained by Frost,[42] whereas only one peak at 1077 cm^{-1} has been found by Farmer.[44] The origin of this relatively large underestimation of the experiment by the simulation is not clear; it cannot be attributed to possibly large anharmonicity effects because, in that case, our harmonic frequencies would overestimate, rather than underestimate, the experiment. The presence of water molecules in the cavities might be invoked to explain the extra rigidity of the OH bending modes. The calculated mode at 1235.2 cm^{-1} is not observed in any experiment; this is not surprising as its intensity is very low.

Regarding the stretching region, many peaks are reported ranging from 2900 to 3600 cm^{-1}, corresponding to OH stretching modes; the highest ones are attributed by the authors to surface OH and to interactions with water. The two peaks that could correspond to the pure OH stretching are at 2910−2995 cm^{-1}, to be compared to the calculated harmonic frequencies at 3159−3166 cm^{-1}, with a difference of 250 and 170 cm^{-1}, respectively. There are two points that require some comments here, (1) the large overestimation of the experiment by theory and (2) the large difference between the two peaks, not reproduced by simulation (85 vs 7 cm^{-1}). With regards to the first point, anharmonicity of the OH stretching modes is mainly responsible. The red shift due to anharmonicity has been estimated and compared to accurate experimental data in cases where OH is not involved in HBs (see Table 1), and its stretching can be treated as an individual mode by computing the total energy along the OH coordinate and numerically solving the one-dimensional Schrödinger equation. In these cases, anharmonicity is as large as 150−180 cm^{-1}. In the present case, where strong HBs are present, this simplified scheme is not very effective; we can however argue that a further red shift of 50−80 cm^{-1} is compatible with the short OH···O distance (see Table 3).

In regards to the second point, in a previous section, it has already been commented that the band formed by the four OH stretching is relatively narrow (28 cm^{-1}) because the distance among the H is large (each H atom has two H neighbors at 2.37 and one at 2.87 Å). We then suspect the experimental data to be effected by a relatively large inaccuracy in this region (remember that in this region, the experimental band is as large as 800 cm^{-1}).

Most of the comments concerning the comparison with IR experiments apply also to Raman data (Table 7), with an important difference; unfortunately, we are not yet able to compute Raman intensities, and therefore, we are unable to decide whether the absence of peaks in the experimental set is due to low intensity or to other reasons.

In Ruan's paper,[18] 28 peaks are reported, more than the 24 symmetry-allowed (probably due to loss of symmetry and large bands). For 15 of the 28 peaks, a one-to-one correspondence with the calculated data has been established; the maximum difference, $|\Delta_{max}|$, is 18.2 cm^{-1}, and $|\bar{\Delta}|$ is 7.2 cm^{-1} in the 150−800 cm^{-1} range of the spectrum (for the OH stretching, the same treatment discussed for the IR spectrum can be applied). Only 8 out of 24 peaks are provided by the Raman Spectra Database of Mineral Inorganic Materials[46] in the range 200−1400 cm^{-1}, 7 of which agree with the calculated values and with the other experiment.[18] The AlOH bending modes, not seen

by experiment, could have a very low intensity, as in the case of the IR; see Table 6. Peaks found between 800 and 1100 cm^{-1} probably correspond to overtones and therefore could be for the bands at 1180 cm^{-1}, whereas peaks over 3200 cm^{-1} (not shown in Table 7) are due to adsorbed water.[18]

References and Notes

(1) Gale, J. D.; Rohl, A. L.; Milman, V.; Warren, M. C. *J. Phys. Chem. B* **2001**, *105*, 10236.

(2) Digne, M.; Sautet, P.; Raybaud, P.; Toulhoat, H.; Artacho, E. *J. Phys. Chem. B* **2002**, *106*, 5155.

(3) Chroneos, A.; Desai, K.; Redfern, S. E.; Zacate, M. O.; Grimes, R. W. *J. Mater. Sci.* **2006**, *41*, 675.

(4) Clarck, G. R.; Rodgers, K. A.; Handerson, G. S. *Z. Kristallogr.* **1998**, *213*, 96.

(5) Kiss, A. B.; Keresztury, G.; Farkas, L. *Spectrochim. Acta, Part A* **1980**, *36*, 653.

(6) Ruan, H. D.; Frost, R. L.; Kloprogge, J. T.; Duong, L. *Spectrochim. Acta, Part A* **2002**, *58*, 265.

(7) Krokidis, X.; Raybaud, P.; Gobichon, A. E.; Rebours, B.; Euzen, P.; Toulhoat, H. *J. Phys. Chem. B* **2001**, *105*, 5121.

(8) Raybaud, P.; Digne, M.; Iftimie, R.; Wellens, W.; Euzen, P.; Toulhoat, H. *J. Catal.* **2001**, *201*, 236.

(9) Digne, M.; Sautet, P.; Raybaud, P.; Euzen, P.; Toulhoat, H. *J. Catal.* **2002**, *211*, 1.

(10) Garcia-Guinea, J.; Correcher, V.; Rubio, J.; Valle-Fuentes, F. *J. Phys. Chem. Solids* **2005**, *66*, 1220.

(11) Chroneos, A.; Ashley, N. J.; Desai, K. H.; Maguire, J. F.; Grimes, R. W. *J. Mater. Sci.* **2007**, *42* (6), 2024.

(12) Wang, S. L.; Johnston, C. T. *Am. Mineral.* **2000**, *85*, 739.

(13) Balan, E.; Lazzeri, M.; Morin, G.; Mauri, F. *Am. Mineral.* **2006**, *91*, 115.

(14) Winkler, B.; Hytha, M.; Pickard, C.; Milman, V.; Warren, M. C.; Segall, M. *Eur. J. Mineral.* **2001**, *13*, 343.

(15) Wolverton, C.; Hass, K. C. *Phys. Rev. B* **2001**, *63*, 024102.

(16) Rosso, K. M.; Rustad, J. R. *Am. Mineral.* **2001**, *86*, 312.

(17) Winkler, B.; Milman, V.; Hennion, B.; Payne, M. C.; Lee, M. H.; Lin, J. S. *Phys. Chem. Miner.* **1995**, *22*, 461.

(18) Ruan, H. D.; Frost, R. L.; Kloprogge, J. T. *J. Raman Spectrosc.* **2001**, *32*, 745.

(19) Saunders, V. R.; Dovesi, R.; Roetti, C.; Orlando, R.; Zicovich-Wilson, C. M.; Harrison, N. M.; Doll, K.; Civalleri, B.; Bush, I. J.; D'Arco, P.; Llunell, M. Crystal 2006 user's manual. www.crystal.unito.it/Manuals/crystal06.pdf.

(20) Crystal web site: examples of graphical animations of vibrational modes. www.crystal.unito.it/prtfreq/jmol.html.

(21) Montanari, B.; Civalleri, B.; Zicovich-Wilson, C. M.; Dovesi, R. *Int. J. Quantum Chem.* **2006**, *106*, 1703.

(22) Pascale, F.; Tosoni, S.; Zicovich-Wilson, C.; Ugliengo, P.; Orlando, R.; Dovesi, R. *Chem. Phys. Lett.* **2004**, *396*, 308.

(23) Orlando, R.; Torres, F. J.; Pascale, F.; Ugliengo, P.; Zicovich-Wilson, C.; Dovesi, R. *J. Phys. Chem. B* **2006**, *110*, 692.

(24) Pascale, F.; Zicovich-Wilson, C. M.; Orlando, R.; Roetti, C.; Ugliengo, P.; Dovesi, R. *J. Phys. Chem. B* **2005**, *109*, 6146.

(25) Prencipe, M.; Pascale, F.; Zicovich-Wilson, C. M.; Saunders, V. R.; Orlando, R.; Dovesi, R. *Phys. Chem. Miner.* **2004**, *31*, 559.

(26) Pascale, F.; Catti, M.; Damin, A.; Orlando, R.; Saunders, V. R.; Dovesi, R. *J. Phys. Chem. B* **2005**, *109*, 6146.

(27) Pascale, F.; Zicovich-Wilson, C. M.; Gejo, F. L.; Civalleri, B.; Orlando, R.; Dovesi, R. *J. Comput. Chem.* **2004**, *25*, 888.

(28) Tosoni, S.; Pascale, F.; Ugliengo, P.; Orlando, R.; Saunders, V. R.; Dovesi, R. *Mol. Phys.* **2005**, *103*, 2549.

(29) Ugliengo, P.; Pascale, F.; Mérawa, M.; Labéguerie, P.; Tosoni, S.; Dovesi, R. *J. Phys. Chem. B* **2004**, *108*, 1362.

(30) Doll, K. *Comput. Phys. Commun.* **2001**, *137*, 74.

(31) Doll, K.; Harrison, N. M.; Saunders, V. R. *Int. J. Quantum Chem.* **2001**, *82*, 1.

(32) Civalleri, B.; D'Arco, P.; Orlando, R.; Saunders, V. R.; Dovesi, R. *Chem. Phys. Lett.* **2001**, *348*, 131.

(33) Schlegel, H. B. *J. Comput. Chem.* **1982**, *3*, 214.

(34) Noel, Y.; Zicovich-Wilson, C.; Civalleri, B.; D'Arco, P.; Dovesi, R. *Phys. Rev. B* **2002**, *65*, 014111.

(35) Zicovich-Wilson, C.; Bert, A.; Roetti, C.; Dovesi, R.; Saunders, V. R. *J. Chem. Phys.* **2002**, *116*, 1120.

(36) Zicovich-Wilson, C.; Dovesi, R.; Saunders, V. R. *J. Chem. Phys.* **2001**, *115*, 9708.

(37) Baranek, P.; Zicovich-Wilson, C.; Roetti, C.; Orlando, R.; Dovesi, R. *Phys. Rev. B* **2001**, *64*, 125102.

(38) Ugliengo, P. Moldraw 2.0, version h1. www.moldraw.unito.it.

(39) 3D animation of diaspore vibrational modes. www.crystal.unito.it/vibs/diaspore.

(40) Jmol website. http://jmol.sourceforge.net/.

(41) Crystal website. www.crystal.unito.it.

(42) Frost, R. L.; Kloprogge, J. T.; Russel, S. C.; Szetu, J. *Appl. Spectrosc.* **1999**, *53*, 829.

(43) Hill, R. J. *Phys. Chem. Miner.* **1979**, *5*, 179.

(44) Farmer, V. C. *Infrared Spectra of Minerals*; The Mineralogical Society: London, 1974.

(45) Stegmann, M. C.; Vivien, D.; Mazieres, C. *Spectrochim. Acta, Part A* **1973**, *29*, 1653.

(46) Raman spectra database of mineral inorganic materials. www.aist.go.jp/RIODB/rasmin/.

(47) Kloprogge, J. T.; Ruan, H. D.; Frost, R. L. *J. Mater. Sci.* **2002**, *37*, 1121.

(48) Koch, W.; Holthausen, M. C. *A Chemist's Guide to Density Functional Theory*; Wiley-VCH: Weinheim, Germany, 2000.